Mid-term report

Quantifying numerical diffusion and dispersion in D-Flow Flexible Mesh usinga lock-exchange experiment

by

D. Koetsenruijter

Student number: 4332601
Project duration: April 20, 2020 – June 12, 2020
Thesis committee: ir. L.M. Keyzer, TU Delft, first supervisor
Prof. dr. J. Pietrzak, TU Delft, second supervisor

TU Delft

Contents

1

Introduction

The salinity of water systems is caused by saltification of a fresh water body. Often fresh water is to remain fresh in order to extract drinking water, for use in agriculture or because of its importance to an ecological system. However in coastal water systems such as the Rhine-Maas delta, mixing of fresh and salt water is inevitable. Since salinity differences cause for density driven currents to occur (see 1.1) and because important water infrastructure in the Netherlands, such as the drinking water supply, is strongly influenced by these currents it is important to understand, model and predict these phenomena. Moreover, salinity in surface waters in the whole European delta is a growing problem given smaller river discharges and a growing demand for fresh water, due to the effects of a changing climate [Friocourt et al., 2014]. This increases the need to accurately model density driven currents caused by salinity differences. With the use of D-Flow Flexible Mesh, a software package by Deltares, such density driven flows can be numerically approximated using 2D and 3D flow modelling. However, a side effect of these numerical flow models is the occurrence of numerical errors caused by characteristics of the discretization scheme that is used and the type of flow that is modelled. Two types of numerical errors that typically occur are numerical diffusion and -dispersion.

This research aims to quantify the numerical diffusion and -dispersion produced by D-Flow FM while modelling salinity transport, using a lock-exchange experiment. This is done by investigating the models' sensitiviy to important numerical parameters such as time step size and grid resolution by means of a sensitiviy analysis.

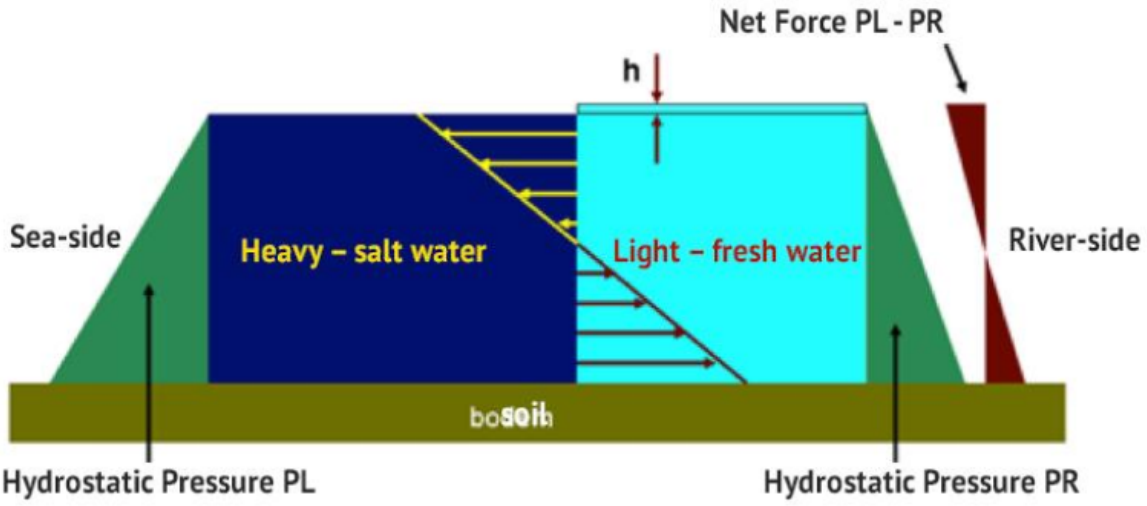

Figure 1.1: Physical model of a density driven current - Source: Friocourt et al. [2014]

Numerical diffusion and -dispersion

Numerical diffusion is sometimes referred to as “numerical viscosity” since the associated approximation errors mimic the effect of an increase in viscosity, i.e. the solution is overdamped. For numerical methods that apply finite-differences in combination with an explicit time integration scheme often this sort of damping is introduced to keep the scheme stable Zijlema [2015, Chapter 3]. Because D-Flow FM applies such a discretization method on the shallow water equations it is important to quantify the effect observed at different configurations.

Numerical dispersion is related to unrealistic oscillations in an approximation of an advection-diffusion problem that may occur when modelling steep gradients causing the model oscillate at locations away from the discontinuity in order to maintain a smooth solution and approximate the sudden steep gradient at the same time.

Because avoiding errors related to numerical diffusion and -dispersion requires contrasting measures [O’Brien et al., 1950] with respect to settings of the numerical model a quantification of their responses to certain modelling parameters is desirable.

A challenge in quantifying these errors arises when modelling flow in which large vertical velocities occur, i.e. in non-laminar flow. If for this sort of flow, which possibly occurs in the lock-exchange experiment,the shallow water equations are used, which is the case in the D-Flow Flexible Mesh flow model, flow related errors can be expected. Thus, because the flow model used also produces errors that are an effect of the assumptions made in the flow model and not of the numerical model used, a clear distinction between these two origins of error should be made.

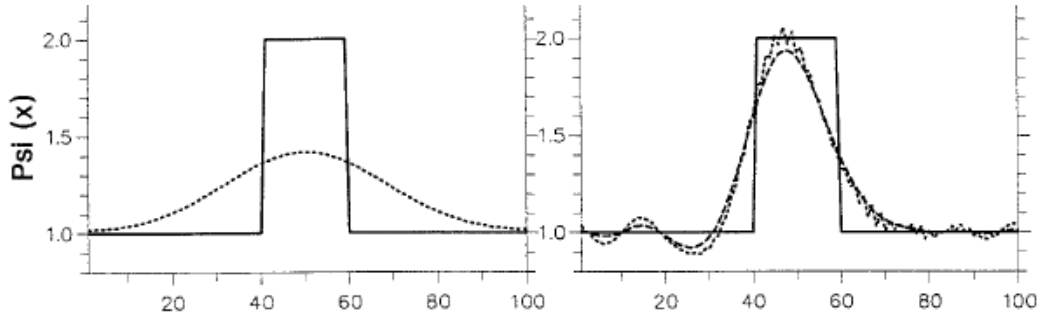

Figure 1.2: Typical examples of numerical diffusion (left) and dispersion (right) in approximating steep gradients - Source: Pietrzak [1998]

Lock-exchange experiment

To be able to refer the sensitivity of numerical errors produced by D-Flow FM to specific settings and parameters of the model a lock-exchange experiment is set up. In a lock-exhange the initial situation consists of a rectangular tank with a horizontal free water surface, for one half containing a fluid with a higher density than on the other half of the fluid tank, split vertically. In this research the density difference is caused by an initial salinity difference. At the start of the experiment ($T = 0$) these fluids set in motion and from two fronts, a low- and high density front, as a result of the gravitiational and buoyant forces (see 1.3). The numerical errors produced during such an experiment have been investigated before of which the results will be compared to the results of this report [Adduce et al., 2012, Cenedese et al., 2018, Shin et al., 2004].

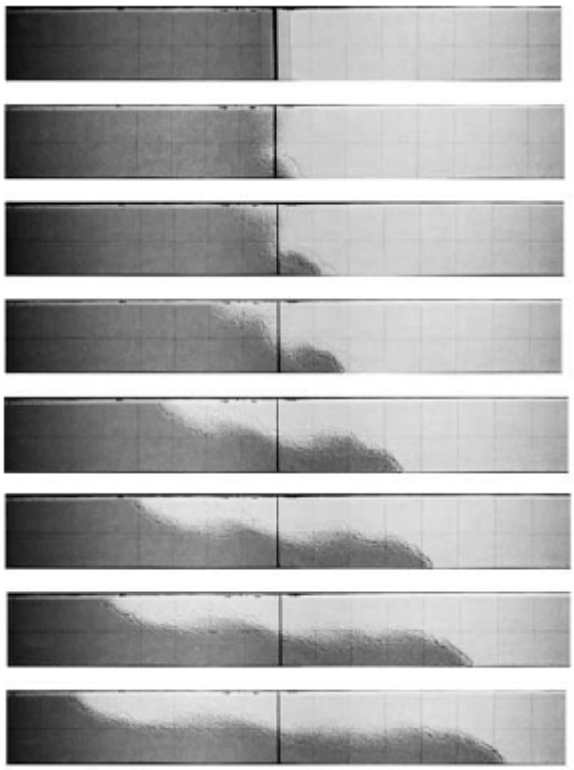

[H]

Figure 1.3: Example of a lock-exchange experiment depicting two current fronts flow opposite directions over time - Source Shin et al. [2004]

This study

In modelling flow and transport phenomena, and numerical modelling in general, two variables have a major effect on the stability and accuracy of the solution; the spatial resolution and time step size. Additionally there are many different other numerical and flow related parameters in D-Flow FM that can be set and might have influence on the numerical errors produced. For further reference see 2 or [Deltares, 2020]. In this study these parameters are varied within relevant ranges during three stages of the simulation phase of this research; temporal variations, variations in spatial resolution and variations of other numerical parameters. Finally the observed sensitivity of the numerical errors per parameter is analyzed, where the sensitivity S of a parameter P is defined as the relative change of a state variable per change of this parameter: $S = (\delta x/x)/(\delta P/P)$. The observed numerical dispersion is quantified by comparing the salinity of a single cell over time at the location of the initial disturbance and at locations where each front is fully developed, to an appropriate reference model. The observed numerical diffusion is quantified as the ratio of the theoretically approximated propagation speed of the front and the observed frontal propagation speed (FPS), for both the high density front (HDF) and low density front (LDF). The quantification of both errors will serve as state variables in the sensitivity analysis.

First, this report describes some background information related to the lock-exchange experiment, to modelling of flow and transport in general and to D-Flow Flexible Mesh in chapter one. Then, in chapter two the methodology used attain the models' sensitivity. In chapter three the results of the simulations with different parameters and the models sensitivity are presented. Finally, in chapter four, conclusions with respect to the models' sensitivity are presented and the obtained results are discussed.

2

Background

Because D-Flow FM implements many complex details of a numerical scheme only a few important aspects are shortly described here. For further elaboration the reader is referred to Appendix B - D-Flow Flexible Mesh or [Deltares, 2020]. D-Flow FM implements the shallow water equations that have as basic assumptions that the vertical velocity is small compared to horizontal scale, the vertical pressure is nearly hydrostatic and wave induced accelerations in the vertical cause negligible effect on the pressure distribution compared to the wave induced height difference. Further the shallow water equations have as property that the water density is directly proportional to bed- and wind friction terms. D-Flow FM uses an finite differences method with an upwind scheme (implicit) to solve the governing equations. Most importantly D-Flow is capable of implementing many sorts of meshgrid types, including triangles, quids, pentagons and hexagons in a curvilinear grid.

TODO: give formulae for shallow water equations, convection equation and numerical model

In general finite differences based methods used to approximate convection-diffusion problems using the shallow water equations, the hydrostatic assumption causes errors related to vertical accelerations that can not be accounted for (i.e. vertical velocity gradients). Because the continuity equation can only account for small variations in the vertical velocity gradient when larger accelerations occur numerical models show physically unrealistic phenomena such as spurious oscillations in salinity profiles and, in the case of the lock-exchange esperiment, smaller propagations speeds of the two density fronts than would be expected based on the energy balance [Pietrzak, 1998]. This is also experimentally confirmed as presented in Simpson and Manga [1998]. Thus depending on the order of velocity varations in the vertical, given a specific timestep size and spatial resolution, the hydrostatic assumption can cause larger or smaller numerical errors. In practice this means the modelled flow should be more or less laminar which allows the solution to be smoothly varying and the continuity equation can account for the vertical velocity variations. Taking this into account, during a lock exchange experiment the largest errors may be expected near the density fronts and near the interface between the two density driven currents, due to respectively steep salinity gradients causing large discontinuities and high shear stresses causing turbulence thus vertical velocity gradient (also known as the Benard-Von Karman instability [Mathis et al., 1984]).

For most flows in a lock exchange, depending mostly on the Reynolds number [Shin et al., 2004], resistance can be ignored. Also described in [Battjes, 2017], when damping of wave amplitude is as little as possible the energy conserving assumption is most valid and uniform flow behind the wavefront can be assumed. By examening the flow based on the above assumptions, numerical errors may also be be recognized at times when the hydrostatic assumption is least valid. For example at t=0 because of the large initial disturbance, when a relatively large velocity gradient between the two sides of each front occurs, numerical dispersion could occur because the model struggles to account for these large gradients. Similarly at times when Benard-Von Karman instabilities are fully developed numerical diffusion may be significant, since the type of numerical models considered tend to flatten out these smaller-scale vertical velocity gradients. Lastly, if the frontal propagation speeds (the propagation velocity of the low- and high density front) does not comply with estimations as proposed by literature [Pietrzak, 1998] it could be an indication of numerical diffusion.

TODO: explain the courant number and other numerical conditions shortly

3

Method

In order to obtain an indication and quantification of the numerical dispersion and -diffusion produced by D-Flow FM, given different parameters are set the following research method is presented.

The method is split in three phases: modelling, simulation and analysis, which respectively comprise the modelling and describing of the frame of reference for each parameter variation, running simulations over a range of values per parameter and analyzing the results using a sensitivity analysis and appropriate indicator parameters. Hereafter the produced results can be discussed and possibly conclusions with respect to the to the research questions can be drawn.

3.1. Modelling the frame of reference

During the modelling phase a frame of reference for the observed errors in the subsequent parameter variations is determined. This frame of reference thus serves as a baseline for the quantification of errors. However, this frame of reference is further developed as different parameter variations are performed. It is therefore split into four different reference models being; the initial-, primary-, secondary- and tertiary reference model.

The initial reference model is determined by exploring D-Flow FM, it's possible settings and thus through experimenting with different parameters that are to remain constant in the further simulations. Based on a qualitative analysis of these results and further reasoning the model settings and parameters that will remain constant throughout the further research are reasonably defined. Because a constant time step size (Δt) is desired for the spatial variations and both temporal and spatial step sizes (Δt, Δx, Δy and Δz) are desired to be constant while varying miscellaneous numerical parameters, the initial reference model develops into the primary-, secondary- and tertiary reference model for respectively the temporal, spatial and miscellaneous parameter variations. Thus after the temporal variations a secondary reference model is defined which uses a constant Δt and can be used for the spatial variations. Then after the spatial variations a tertiary reference model is defined, in which a constant Δx, Δz and $Gridmeshtype$ are set on top of the constant Δt. Then finally the advection type, advection- and salinity limiter types are varied and compared to the tertiary reference model.

In all reference models the observed numerical dispersion and -diffusion should be minimized and clearly recognizable. With respect to the secondary and tertiary reference model, an extra requirement is that the time step size and spatial resolution in the x-direction should allow the subsequent parameter variations to be varied over the range of Courant numbers that is of interest. This range of Courant numbers is defined as follows: $C \in [0.1, 2]$, however also extreme values ($C = 0.01$ or $C = 5$) are of interest.

Initial reference model

For the initial reference model most default settings are used to set up the lock-exchange model. Besides, the boundary conditions are determined to be free-slip for all sides of the watertank and prescribe a zero-discharge condition. The water tank is defined to be 100 meters wide, 10 kilometers long, has a depth of 10 meters and every simulation spans a period of 5 hours. The geometry is descretized by a computational grid with 100 cells of of 100 meters, 3 cells of 100 meters and 10 cells of 1 meter in

x-, y- and z-direction respectively. Finally it is noted that the background temperature is set to be 10 degrees Celsius, which is not default but more conventional than the default 6 degrees Celsius.

First a qualitative assessment of this initial reference model is made which takes a few iterations of temperature and number of layers in the z-direction. With respect to post-processing the initial reference model two parameters are evaluated; the width averaged water level over time, because of its simple nature, and the width averaged salinity over time because of its clear relevance. The first in a single plot and the latter in 5 subplots. For the salinity profiles points where they either have an extreme (physically unrealistic) value are After basic post processing these variations the results and the complete settings of the intitial reference model are presented in C. Based upon this well-focused observations can be made in the subsequent simulations. As all desirably constant parameters are defined the primary reference model is thus defined and can be used for the temporal variations.

Primary-, secondary and tertiary reference model

Below the settings for all reference models are presented. Since the reference models form the basis for the parameter variations, it may be clear that after the temporal variations the time step size becomes a constant variable and after the spatial variations the resolution in all directions is also kept constant, respectively producing the secondary an tertiary model.

Parameters / Reference model	Unit	Primary	Secondary	Tertiary
Geometry				
# Grids - M	-	100	100	
# Grids - N	-	3	3	
Delta x	m	100	100	
Delta y	m	100	100	
General				
# Layers	-	10	10	
Timeframe				
Period	s	18000	18000	
Courant number	-	0.7	1200	
max. time step	s	1200	60	
Initial time step	s	1	60	
Processes				
Salinity	ppt	TRUE	TRUE	
Initial conditions				
Waterlevel	m	10	10	
Salinity delta	ppt	25-15	25-15	
Temperature	degC	10	10	
Boundary conditions				
Discharge	m3/s	TRUE	TRUE	
Velocity	m/s	FALSE	FALSE	
Type	-	Free-slip	Free-slip	

Table 3.1: D-Flow Flexible Mesh settings defined for the primary reference model

3.2. Simulations

In order to generate the data required for the sensitivity analysis a number of simulations have to be performed. By varying the different parameters the associated numerical errors can be computed. Because this is done over a realistic and relevant range of values, the numerical diffusion and -dispersion errors generally produced by D-Flow FM can be quantified.

Three sets of parameter variations will be performed. First, the temporal variations consisting of Δt and the $Courant_{max}$ are performed and compared to the primary reference model. Second, the spatial variations consisting of Δx, Δz and $Gridmeshtype$ are performed and compared to the secondary reference model. Last, miscellaneous numerical parameters are varied and compared to the tertiary reference model.

Quantification of errors

The simulations are compared according to the quantification of the observed numerical diffusion and -dispersion. Numerical diffusion is quantified using the ratio between observed- and theoretical frontal propagation speed at both fronts. Where the theoretical frontal propagation speed is estimated by the following formulas, as used by [Pietrzak, 1998] and confirmed through experiment by Simpson and Manga [1998], based on the energy conserving nature of gravity induced currents in long prismatic channels.

$$U = C_{front} \cdot \sqrt{(g' \cdot d)}$$

With:

$$g' = g(\rho_2 - \rho_1)/\rho_2$$

Given that:

$$\rho_1 < \rho_2$$

And:

$$\begin{cases} C_{front} = 0.44, & \text{for the high density front} \\ C_{front} = 0.56, & \text{for the low density front} \end{cases}$$

The numerical dispersion is quantified by plotting the salinity of a single cell over time, at a depth and points where maximum dispersion errors are expected, for both the low density front and the high density front. In order to observe the effect of both the fully developed fronts (travelling in opposite directions) and to get insight in what happens after $t = 0$ at the location of the initial disturbance, these points are at the location of the initial salinity difference ($x = 5000$) and at locations where the fronts are fully developed as they reach the location ($x = 2500$ for the LDF and at $x = 7500$ for the HDF), which follow from inspection of the initial- and primary reference model. The salinity at the beforementioned locations are then plotted and compared to the respective reference model from which a salinity difference can be calculated. This salinity difference is thus relative to the respective reference model and serves as the measure for numerical dispersion.

3.2.1. Parameter variations

For the parameter variations the sequential order matters as it is desirable to have a constant time step for all subsequent variations. Therefore it is important to have investigated the effect of the automatic time step setting implemented by D-Flow FM based on the maximum Courant number ($Courant_{max}$) and a range of constant time step sizes (Δt) before defining a constant time step size for the secondary reference model. With similar reasoning a logical spatial resolution (Δx, Δz and $Gridmeshtype$) should be chosen before the type of advection scheme and possible limiters are varied. Because the Courant number plays an important role in computational fluid dynamics it serves as an important measure in the subsequent variations and also serves as a normalization to the range of values over which the temporal and spatial parameters are varied. In table 3.2 the ranges of all performed variations are listed.

Temporal varations

First, simulations with a varying Courant number are performed while using the automatic time step setting in D-Flow FM (see appendix A). These first results are examined and compared to the primary reference model. Hereafter Δt is set constant over a single simulation and it's size is varied, which gives the variation of the time step size parameter. This is only possible if the $Courant_{max}$ parameter is set sufficiently high so that the automatic time step size setting of D-Flow FM does not take effect. By the means of these results a constant time step size for the next parameter variations is chosen to be 60 seconds. Herewith the secondary reference model for the spatial variations is thus obtained.

Spatial variations

Next, the spatial resolution is varied and examined. Although the number of layers is prematurely examined in the reference model both Δx and Δz are varied. This is initially done for the default rectangular shaped meshgrid and afterwards for different types of meshgrid, including triangles, quids, pentagons and hexagons. Then the tertiary reference model can be defined.

Advection type- and limiter types variations

Finally the advection type, advection velocity limiter type and the salinity transport limiter type are varied according to the table below. The results are compared to the tertiary reference model.

Table 3.2: Range of values for temporal and spatial parameter variations

Parameter	***Max. Courant [-]***	***Time step size [s]***	***Delta x [m]***	***Delta z [m]***
Low	0,1	0,1	5	0,1
Courant nr. estimate	0,1	0,0005	6	-
High	2	1000	400	5
Courant nr. estimate	2	5	0,075	-

3.3. Data analysis

The data analysis consists of a qualitative analysis of the results and accordingly a just quantification of the observed errors in order for the errors to be used in the sensitivity analysis. During the qualitative analysis the results of all the post processing of the different performed experiments are analyzed and a relation between the sensitiviy of the observed numerical errors to the change in certain parameters are sought for, either physically or numerically.

After quantifying numerical diffusion and -dispersion per simulation they are compared per parameter. Firstly, by plotting the Courant numbers at the low density front and the high density front versus the diffusion rates of these fronts. After which regression of the observed values of the diffusion rate that can be reasonably taken into account (i.e. that are produced by simulations with reasonably accurate results) points out possible trends per parameter

Secondly, by looking at the standard deviation of the quantification numerical dispersion produced per parameter variation, the relative change of the these errors per parameter variation can be visualized and quantified. Because the parameters were changed over different ranges of values with different units, this quantification per parameter has to be normalized to their relative change in order to be comparable to one another. To this end, based on the quantification of the standard deviation per parameter, a sensitivity analysis is performed. Where the sensitivity of a parameter S(P) is defined as the relative change of the quantified numerical dispersion per change of this parameter:

$$S = \frac{\frac{\delta x}{x}}{\frac{\delta P}{P}}$$

Where the state variable S is thus defined as the quantified numerical dispersion. However, for the time step size and resolution in x-direction the Courant number already indicates for which range of values the errors produced by these two parameters can be compared.

4

Results

The results obtained from running different simulations are presented in the following chapter. **WHAT ARE THESE RESULTS? SUMMARIZE HERE IN TWO OR THREE SENTENCES**

First the results of the modelling phase are presented in which the basic parameters of the model are explored using an initial reference model consisting of a vertically 10-layered grid of 3×100 cells in the horizontal with an initial salinity difference of 10 ppt. (15 ppt. for the low density side and 25 ppt. for the high density side of the model). As a result of this exploration the primary reference model is defined and presented. Second, the results of the temporal variations (Δt and the $Max.Courantnumber$) are described after which a secondary reference model with a constant time step size is defined and presented. Third, using the secondary reference model, the results of the spatial variations (Δx, Δz and $Gridmeshtype$) are presented. Then based on the observed numerical errors and the influence of the different temporal and spatial parameters on these errors, first conclusions about the sensitiviy of the model's accuracy to these basic numerical parameters are presented. Fourth, a tertiary reference model with a constant time step size, a constant spatial variation in x- and z-direction and a constant grid mesh type is described. Using the tertiary reference model the results of variations of remaining miscellaneous numerical parameters such as the type of advection scheme- and/or limiter are presented. Finally conclusions with respect to the model's sensitivity to these remaining parameters are presented and compared to the model's sensitivity to basic numerical parameters.

4.1. Modelling

As a first exploration a few models were run with a single layer in the vertical direction, then a basic model with 10 layers was run and two output parameters averaged over the width were compared over time: the waterlevel and the salinity. Subsequently two sets of parameters were changed, temperature (T) and number of layers in the z-direction (Δz), in order to gain a basic insight in the model's response. With an initial salinity difference of $10ppt.$, a grid consisting of 100x3 rectangular cells and a simulation period of 4 hours some basic observations were made whilst comparing the results to the initial reference model. The specific settings of the initial reference model can be found in appendix C. By varying the temperature from $T = 0$ to $T = 15$ and the vertical resolution from $\Delta z = 1$ to $\Delta z = 1/100$ the following was inferred:

- The frontal propagation speed of both fronts are always linear over time. This indicates an energy conserving approximation as assumed in the theoretical estimation of the frontal propagation speed for both the low- and high density fronts as proposed by Pietrzak [1998].
- The frontal propagation speed in the high density wave is lower than in the low density front. This is because of the bed friction and coincides with experiments performed by Simpson and Manga [1998].
- The temperature has a significant influence on the observed frontal propagation speed. This can be explained through the formula that estimates the frontal wavespeed based on the density difference and the waterdepth. Also as the temperature increased, causing the density of water

to decrease, the frontal propagation speeds could be seen to increase. This coincides with the physics that suggests a larger influence of the salinity difference on the density difference at lower water densities.

- The frontal propagation speed for the low density front seems to increase as Δz decreases, for the high density front it remains almost the same.

- Both the frontal propagation speeds are smaller than the proposed theoretically estimated value which suggests the occurence numerical diffusion.

- The plotted waterlevel shows spurious oscillations which could be dedicated to hydrostatic assumption of the model, to the occurence of artificial viscosity or to numerical dispersion. This requires further investigation.

Thus concluding that computation times were all within reasonable limits while the number of layers in the z-direction reached it's limit at 99, while obtaining results that coincide with the expected physics and numerical diffusion and dispersion are possibly observed. However to obtain better insight in what causes the observed phenomena and how these relate to the numerical accuracy of the model more information is required.

Further, given these observations and building on the explorative initial reference model, the primary reference model is defined. It consists of a grid of 100×3 cells in the horizontal and 10 in the vertical since this gave results reasonably consistent with the physics that may be expected in a lock-exchange experiment. It is set to maintain a constant background temperature of 10 degrees Celsius, run over a period of 5 hours (18000 seconds) and maintain a maximum Courant number of 0.7. It only accounts for salinity transport processes and uses a monotonized central limiter type [Leer, 1977]. The most important settings are summarized in Table 3.1.

4.1.1. Primary reference model

The primary reference model serves as a first indication and quantification for the type and order of the numerical errors of interest. Therefore, by post processing the results of the reference model into different type of plots better insight in the produced approximation and thus the produced errors is obtained. This is initially done by looking at three basic plots of the computed salinity. Thereafter, based on these insights, initial conclusions with respect to the type of error are described.

In figure 4.1 a plot of the width averaged salinity over time is shown, for the complete domain of the experiment defined as $x \in [0, 10000]m$ depicting theoretical and observed frontal propagation speeds for both fronts, unrealistic extreme values (i.e. values where the $sal. \notin [15, 25]$, given that $[15, 25]$ is the range of the initial condition). With the goal of getting an overview of the experiment and it's global numerical diffusive and -dispersive characteristics. As a first observation the development of the front can clearly be seen, a linear propagation speed of both fronts and an increase of the mixing layer over time are also observed. Further no value significanly outside the initial salinity range of $[15, 25]$ is produced by the model otherwise these would have been plotted as a red or a blue dot. Further the theoretically estimated and observed locations of the front are plotted as a normal- and dashed line respectively. The location of the fronts are determined by looking at the lowest and highest value of x, for the low- and high density respectively, for which the absolute the salinity gradient maximized over the depth exceeds 0.1 ppt/m. The mixing layer of the front can be seen to expand as time increases upto width of around 200 meters. Because of this the velocity observed within 200 meters of the location of the front, extending towards the tail of the density gradient, is used to calculate the Courant number at the front which is finally used while plotting the diffusion.

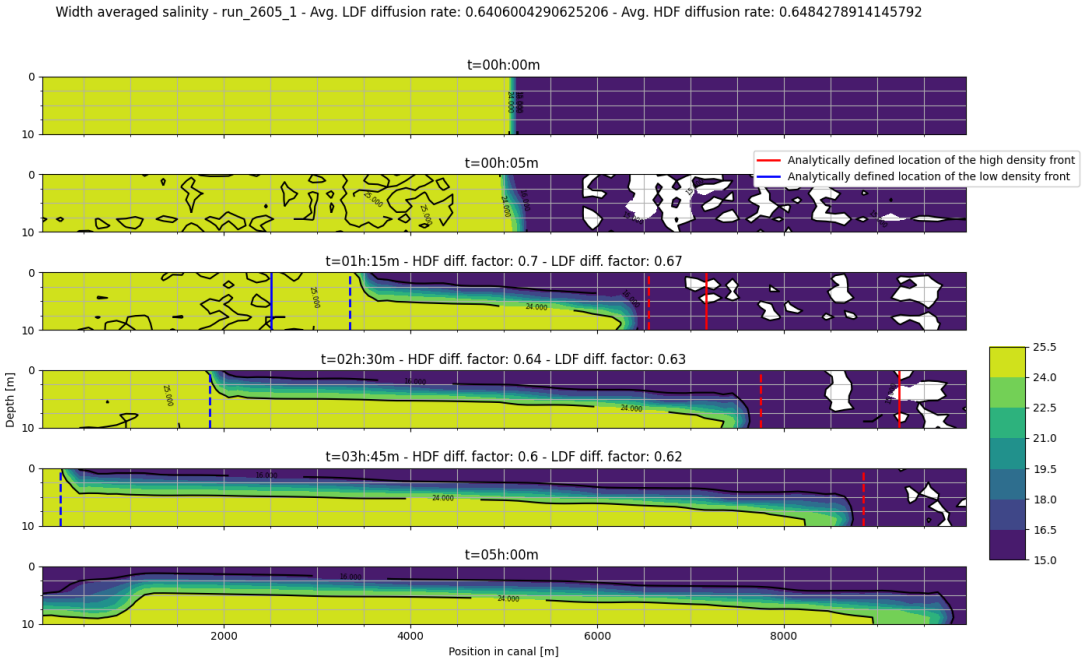

Figure 4.1: Contour plot of the salinity over time for the primary reference model

In figure 4.2 a detailed plot of both fronts and the observed Courant numbers at the front are presented. The plot depicts the situation at $t = 2.5h$ such that the fronts are fully developed, aimed at gaining insight in how oscillations in the salinity profile close to the propagating disturbance develop. The oscillations at the trailing part of the front are expected to be natural and no direct dispersion errors (e.g. in the form of clearly spurious oscillations) are observed in front of the large density gradient. Lastly the Courant numbers are surprisingly low for a $Courant_{max}$ that equals 0.7. Therewith, as a confirmation that the characteristics of the front are captured within of 200m the maximum Courant numbers indeed occur within this range. This can be deduced from figure 4.3 in which the maximum velocity over the depth is used to calculated the Courant number for all locations, moreover the maximum Courant numbers are observed at $t = 2.5h$ thus being a justification for choosing this timestep to inspect in further detail.

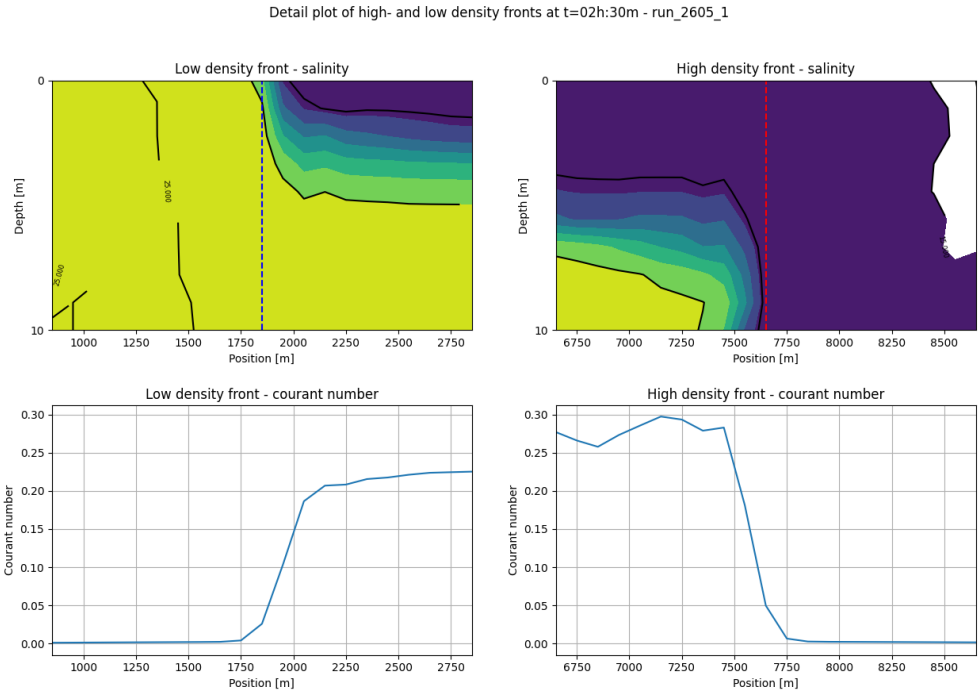

Figure 4.2: Detailed plot of the density fronts produced by the primary reference model

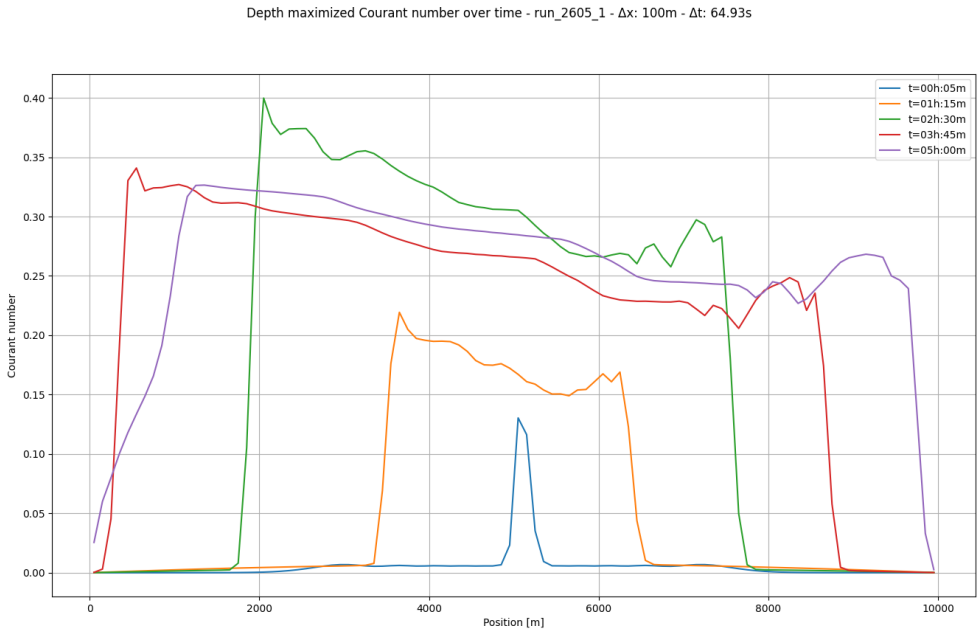

Figure 4.3: Depth maximized Courant number over time

Finally, in figure 4.4 a plot is presented that depicts the salinity at a single cell at three locations, being $x = 2550$, $x = 5050$ and $x = 7650$, used to get an indication of the behaviour of the approximated salinity over time as the front passes. The data that is plotted here is also used to quantify the observed dispersion compared to the reference model. The most important observation is that the maximum gradient occurs at different depths per front. Because at these large gradients the highest numerical

errors are expected these are maintained as the depths at which numerical dispersion is quantified, being; at a depth of 4.5 meter for the middle of domain, 2.5 meter for the low density front and 6.5 meter for the high density front.

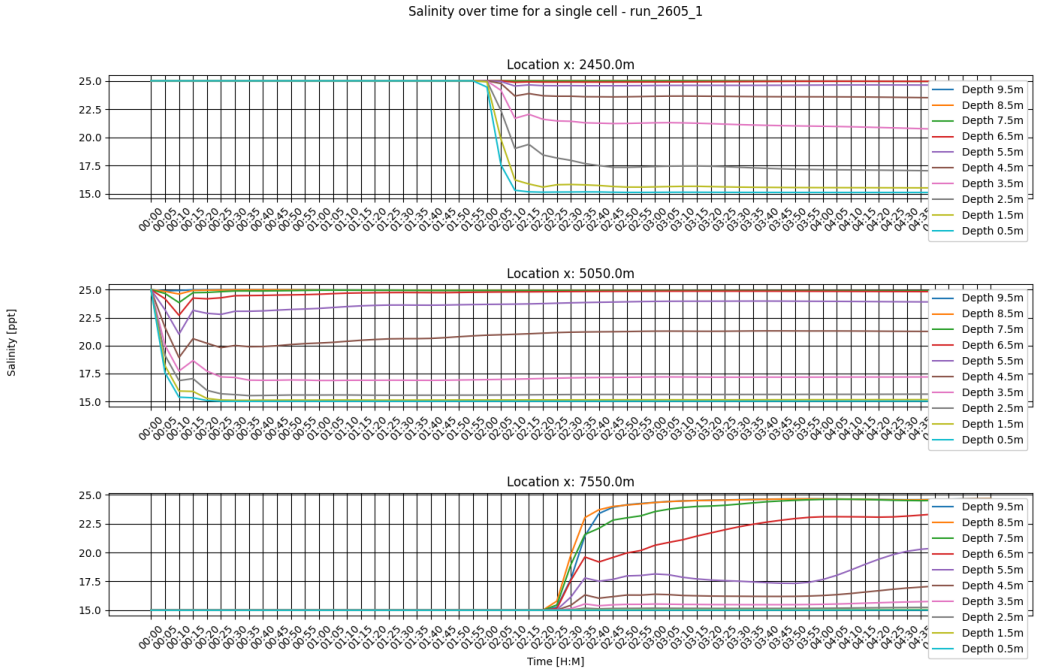

Figure 4.4: Salinity of a single cell at different depths and three locations over time

4.2. Parameter variations

Here the results per parameter variation will be presented mainly by means of the salinity profiles of a single cell at specific depths and locations for all values of the parameter. Therewith these salinities over time are substracted from the reference model after which a relative difference is obtained. This difference is subsequently used to quantify the numerical dispersion observed for the range of parameter values. The data produced with respect to the numerical diffusion will only be presented in chapter 4.3 and in appendix **??**.

4.2.1. Variation of $Courant_{max}$

In figure 4.5 the initial disturbance can clearly be seen to decrease almost immediately (after approximately 600 seconds) to a salinity value of 18 ppt, then after a small oscillation it soon decreases to it's steady state value of approximately 17 ppt. What the origin of this steep oscillation is is yet unclear, however, for all values of Max. Courant the model produces such an error so it is either a numerical error with it's origin in a different parameter or it is an error related to the flow model. Besides, the salinity differences produced after $t = 600$ are of relatively small scale compared to those observed at the low density front in figure 4.6. Passing of the LDF can clearly be observed and the salinity differences are of quite large values. Especially for Max. Courant numbers between 1.6 and 2.0 the effect of the parameter can clearly be observed; as the Max. Courant number increases the model can increase the time step size further and thus increases the range over which possible errors truncate. When such an error truncates over a part of the model where in space and time a large gradient has to be modelled this local truncation error is thus transformed into a large global truncation error. This can be observed in the red and purple salinity profiles that continu far longer at a value of 25 ppt than the other profiles. Since the Courant number can be seen as the ratio between the update speed and the speed at which disturbances travel, the model simply updates faster than the density gradient travels and thus overshoots more as the Max. Courant number increases above 1.0. Further it can be noted that for very small values of Max. Courant the solution does not change much compared to the reference model, it merely responds a little smoother as can be seen in the top plot of figure 4.6. Lastly in figure 4.7 a

larger oscillation as the front has long passed can be seen to slowly develop, possibly related to shear induced Bernard-Von Karman instabilities causing vertical velocities that can not be accounted for in the flow model.

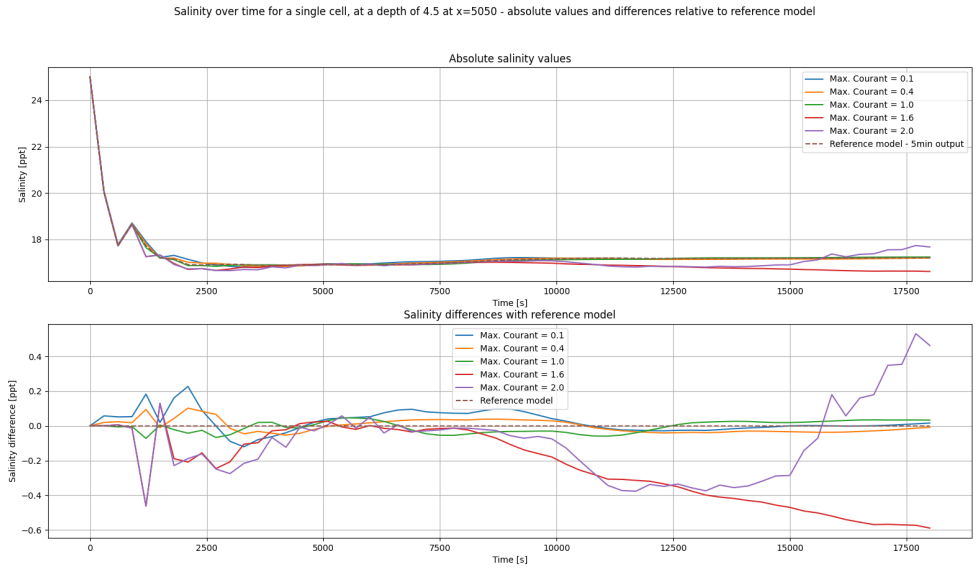

Figure 4.5: Salinity of a single cell at $d = 4.5m$ at the location of the initial salinity difference

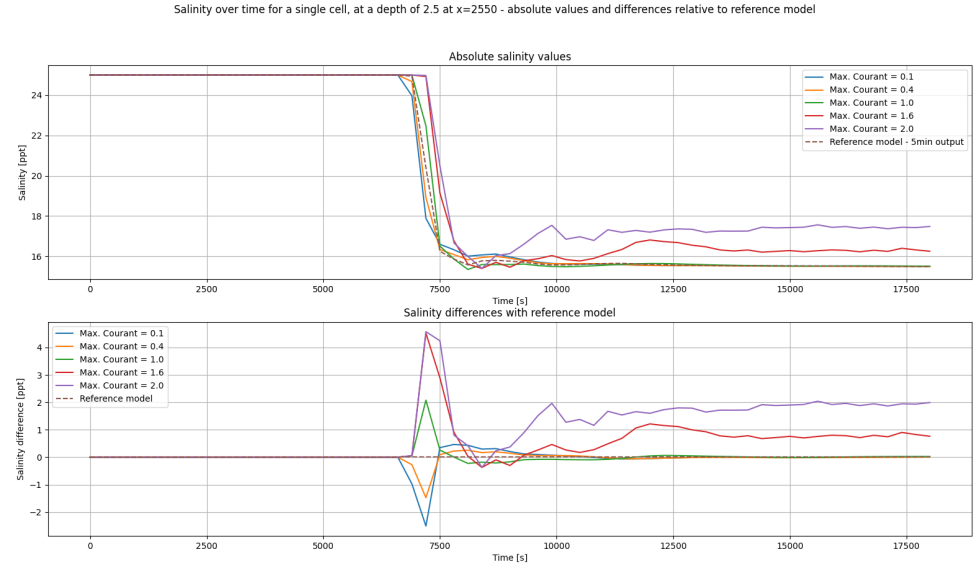

Figure 4.6: Salinity of a single cell at $d = 2.5m$ showing the low density front passing

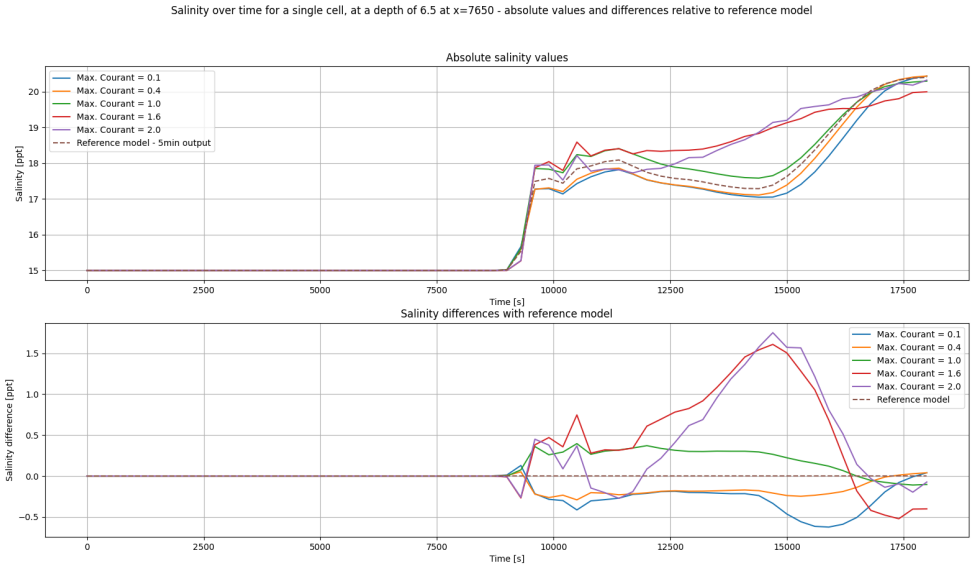

Figure 4.7: Salinity of a single cell at $d = 6.5m$ showing the high density front passing

Variation of Δt

In figure 4.8 clear oscillations can be seen as Δt increases to 250 seconds. Although the absolute error is of a smaller value than at high values of $Courant_{max}$ the characteristics of the oscillation indicate that at steep gradients and a large enough time step size spurious oscillations between the fronts occur. These oscillations start to develop at $\Delta t = 50s$, given a maximum observed velocity of around 0.5 m/s and a Δx of 100m this gives a Courant number of 0.25 which is much lower than expected yet coincides with values found in the primary reference model (see figure **??**). Further figure 4.9 shows the same kind and magnitude of errors as observed in the variations of $Courant_{max}$ as the time step size increases. Lastly spurious oscillations on a smaller scale can be seen to develop at large time step sizes after the high density front has passed (see figure 4.10). As no steep gradient is to be approximated no numerical oscillations are expected. This indicates that indeed small scale vertical velocities the hydrostatic model can not deal with are the cause of the errors in this region of the domain.

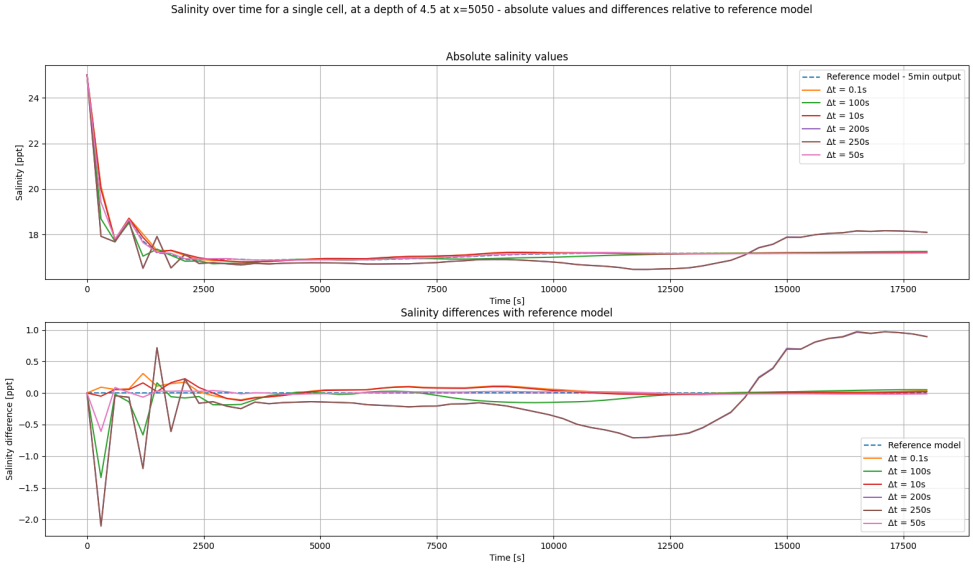

Figure 4.8: Salinity of a single cell at $d = 4.5m$ at the location of the initial salinity difference

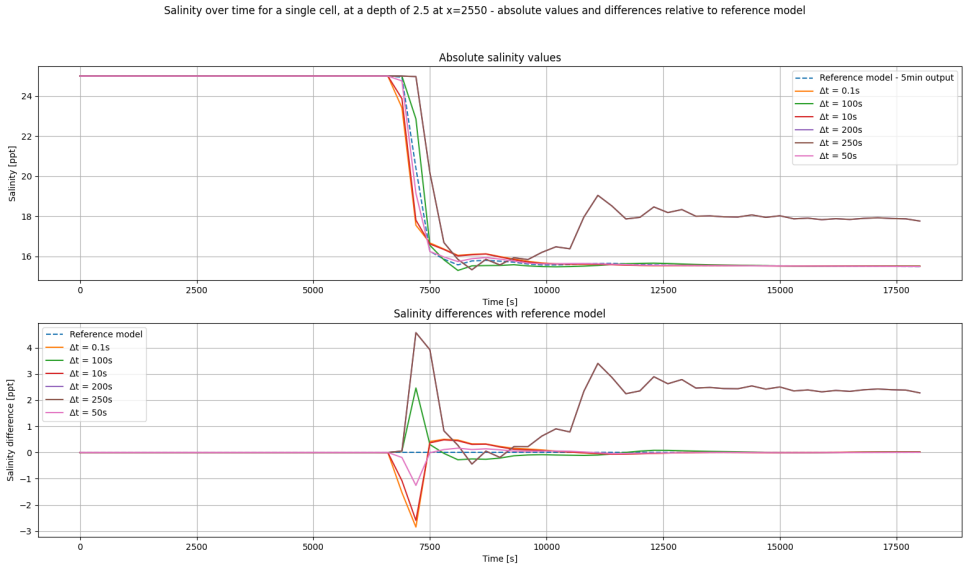

Figure 4.9: Salinity of a single cell at $d = 2.5m$ showing the low density front passing

Figure 4.10: Salinity of a single cell at $d = 6.5m$ showing the high density front passing

Variation of Δx
Variation of Δz
Variation of gridmesh type
Advection type
Advection velocity limiter type
Salinity transport limiter type

4.3. Sensitivity analysis

Next, by comparing the produced salinity profiles for different parameters, conclusions with respect to the sensitivity and order of the produced errors per parameter are drawn.

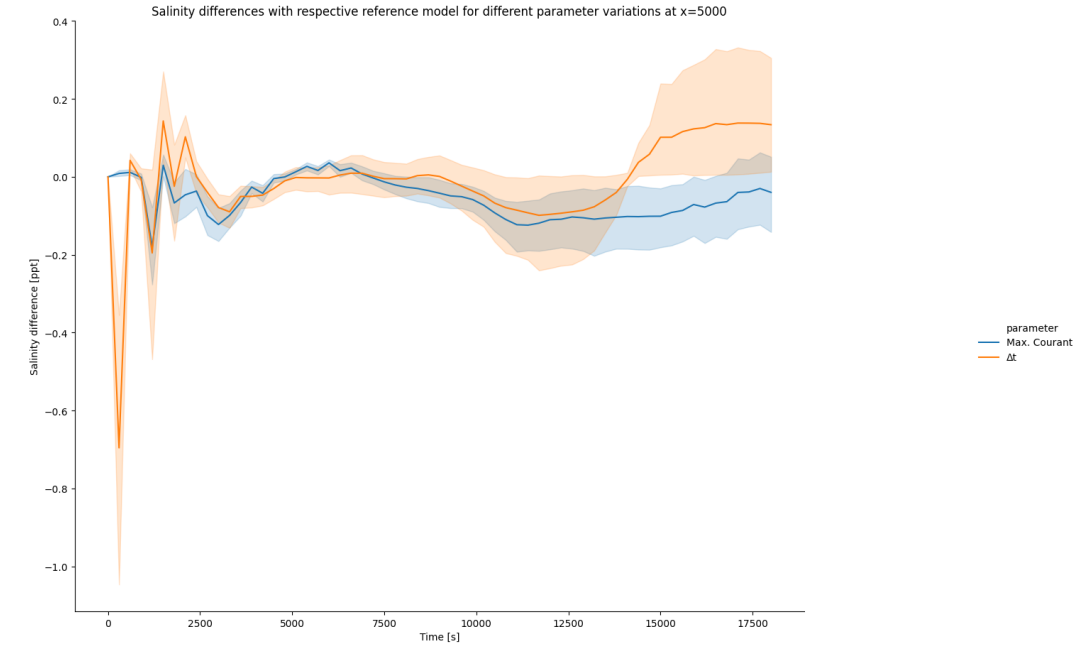

Figure 4.11

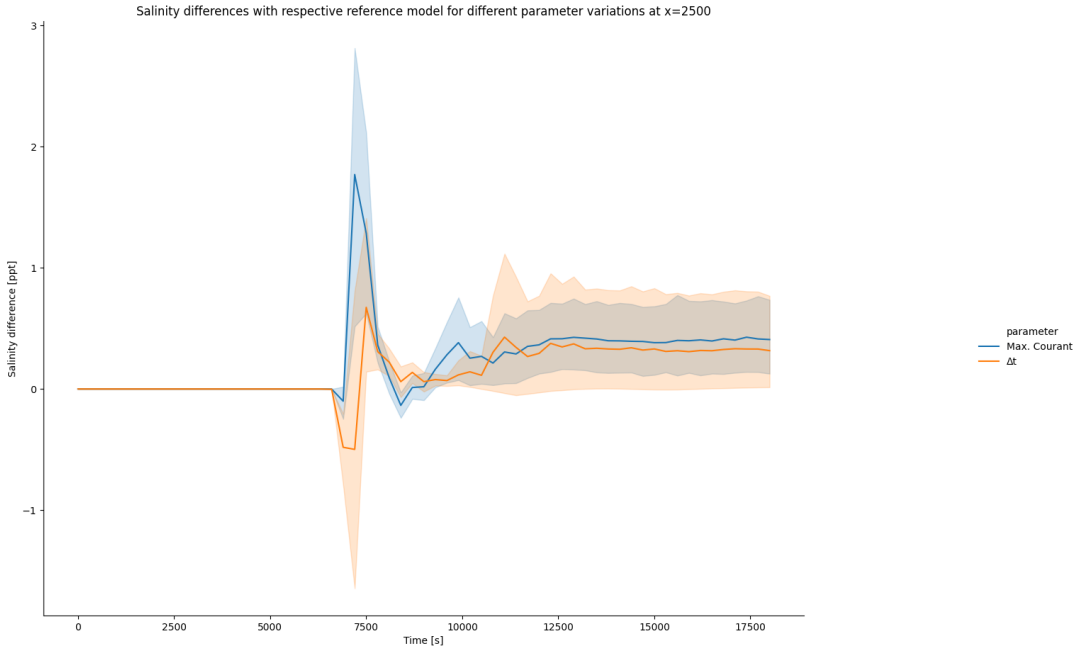

Figure 4.12

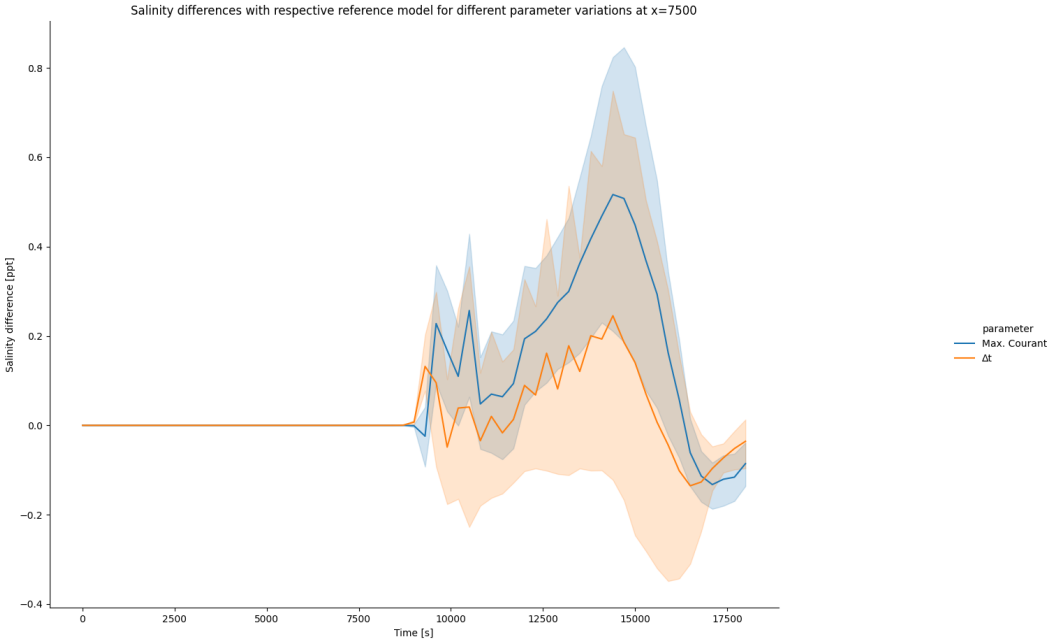

Figure 4.13

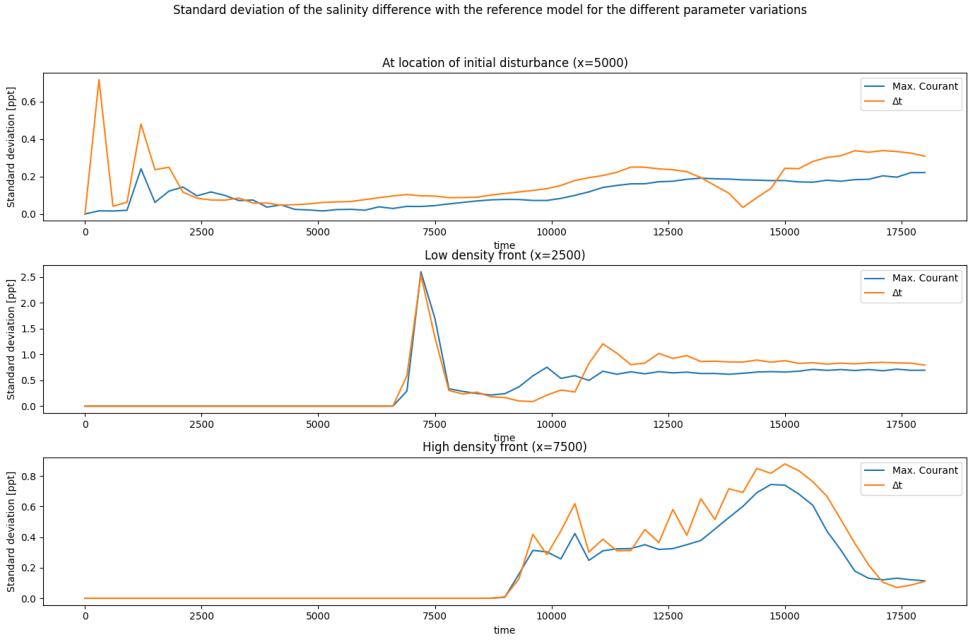

Figure 4.14

5

Discussion and conclusion

Final discussion of the results, their applicability and final conclusions are presented here.

5.1. Conclusion

5.2. Discussion

TODO: Discussion material

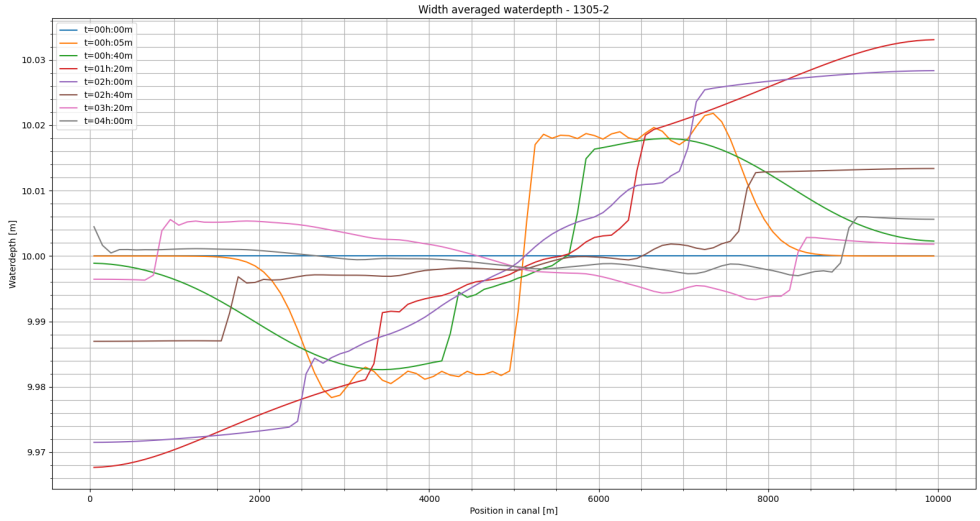

Figure 5.1: Waterlevel - Width averaged waterlevel over time for T=10 degrees Celsius

As to the waterlevel the following can be said:

When the temperature is higher, in the first timestep, oscillations in the waterprofile can be seen in front of the disturbance, besides a large discontinuity around the center of the grid is observed. The fact that these oscillations are not observed at a temperature of 6 degC can be explained due to the relative effect the salinity difference has on the initial density difference, because this effect is smaller at lower temperatures due to a higher density of the water itself the disturbance is of a lower order than at higher temperature. These oscillations are could be a form of numerical dispersion and may be attributed to the hydrostatic assumption of the model, i.e. to compensate for the large vertical velocity gradient in the center of the grid at t=5min the model imposes a waterlevel difference (the large discontinuity). Subsequently to deal with this waterlevel difference in the middle of the grid, the approximation shows

oscillations, i.e. in order to bridge the discontinuity in the waterlevel and approximate the original waterlevel at locations where the disturbance has not yet had any influence. Other oscillations are observed after the wavefronts (especially the high density wave) has passed. These oscillations could be a result of the artificial viscosity of the model, a process imposed to mimick energy loss due to heat transfer, this results in a transfer of kinetic energy in the form of waves. However, they could also be a result of the internal waves formed due to friction at the interface of the two density currents. Because in this mixing layer turbulence is likely to occur the model could show oscillations in the waterlevel to compensate for the vertical velocity gradients associated with turbulence. Because the temperature difference has an indirect effect on the forcing it is desirable to keep this at a constant level and try out a range of different salinity deltas. With this reasoning a default temperature of 4 degrees Celsius should be sustained. A final check in 1305-4 where a background temperature of 0 degrees Celsius, shows similar results as obtained from 1305-2 where a temperature of 10 degrees Celsius was set. Given that the density of water at 0 degrees (9998.7 kg/m³) and 10 degrees (9997.5 kg/m³) are similar, this substantiates this similarity. Finally the results obtained in a situation with 4 degree Celsius is presented.

Spurious oscillations are observed during all simulations at t=5min to deal with the initial disturbance in the waterlevel. This initial disturbance originates from the model's hydrostatic condition and the large vertical velocity gradients at the start of the simulation. Numerical diffusion is possibly observed near the interface of the two density currents. In this mixing layer where turbulunce due to increased shear stresses is expected and clear oscillations are observed when the number of layers is 10. At a higher vertical resolution these short oscillations become a large oscillation with a single wavelenght stretching the grid. This transformation could be a result of the ratio between the horizontal and vertical resolution (1/1000 and 1/100 for 99 and 10 layers respectively) causing different modes in the approximation to be emphasized while trying to account for turbulence in the mising layer. The higher resolution, in simulations with more layers, cause more oscillations in the salinity contour lines to be visible near the front. These small oscillations are expected to be numerically diffused turbulence that may be expected at the progressing wavefronts.

Bibliography

C Adduce, G Sciortino, and S Proietti. Gravity currents produced by lock exchanges: experiments and simulations with a two-layer shallow-water model with entrainment. *Journal of Hydraulic Engineering*, 138(2):111–121, 2012.

Jurjen A. Battjes. *Unsteady Flow in Open Channels*. CAMBRIDGE UNIVERSITY PRESS, 2017. ISBN 1107150299. URL https://www.ebook.de/de/product/27503143/jurjen_a_battjes_unsteady_flow_in_open_channels.html.

C Cenedese, R Nokes, and J Hyatt. Lock-exchange gravity currents over rough bottoms. *Environmental Fluid Mechanics*, 18(1):59–73, 2018.

Deltares. *Technical Reference Manual D-Flow FM*. Deltares systems, version 1.1.0 - svn revision 66571 edition, April 2020.

Y Friocourt, K Kuijper, and N Leung. Salt intrusion. *Deltafacts*, 2014.

Bram Van Leer. Towards the ultimate conservative difference scheme. IV. a new approach to numerical convection. *Journal of Computational Physics*, 23(3):276–299, mar 1977. doi: 10.1016/0021-9991(77)90095-x.

C. Mathis, M. Provansal, and L. Boyer. The benard-von karman instability : an experimental study near the threshold. *Journal de Physique Lettres*, 45(10):483–491, 1984. doi: 10.1051/jphyslet:019840045010048300.

George G. O'Brien, Morton A. Hyman, and Sidney Kaplan. A Study of the Numerical Solution of Partial Differential Equations. *Journal of Mathematics and Physics*, 29(1-4):223–251, 1950. ISSN 1467-9590. doi: 10.1002/sapm1950291223. URL https://onlinelibrary.wiley.com/doi/abs/10.1002/sapm1950291223.

Julie Pietrzak. The use of TVD limiters for forward-in-time upstream-biased advection schemes in ocean modeling. *Monthly Weather Review*, 126(3):812–830, mar 1998. doi: 10.1175/1520-0493(1998)126<0812:tuotlf>2.0.co;2.

L. Prandtl. 7. bericht über untersuchungen zur ausgebildeten turbulenz. 5:136–139, 1925. ISSN 0044-2267. doi: 10.1002/zamm.19250050212.

JO Shin, SB Dalziel, and PF Linden. Gravity currents produced by lock exchange. *Journal of Fluid Mechanics*, 521:1–34, 2004.

John E. Simpson and Michael Manga. Gravity currents in the environment and the laboratory. 51: 70–72, 1998. ISSN 0031-9228. doi: 10.1063/1.882214.

Cornelis Vuik, Fredericus Johannes Vermolen, Martin Bastiaan Gijzen, and MJ Vuik. *Numerical Methods for Ordinary differential equations*. VSSD, 2007.

M. Zijlema. Computational Modelling of Flow and Transport. *Collegedictaat CIE4340*, 2015. URL https://repository.tudelft.nl/islandora/object/uuid%3A5e7dac47-0159-4af3-b1d8-32d37d2a8406.

A

Turbulence modelling in D-Flow FM

A.1. Horizontal eddy viscosity

Modelling horizontal eddy viscosity has three seperate parameters that determine the total viscosity as follow: μ-H = μ-sgs + μ-v + μ-H-back.

These three parameters account for the following: 1. Horizontal turbulent viscosity may be underestimated because of the sub-grid scale turbulent motions, i.e. turbulence on a scale smaller than the meshgrid. This can be resolved by the sub-grid scale viscosity: μ-sgs 2. With Reynolds averaged shallow water equations horizontal eddy viscosity might not accounted for (enough) either thus D-Flow introduces the μ-v. 3. If extra constant or spatially dependant viscosity is desired the background viscosity μ-back may be added.

With respect to the 3D viscosity resulting from three-dimensional turbulence a closure model is used [Deltares, 2020, p.26]. For specific closure models one can even account for unresolved mixing through an ambient background mixing coefficient μ-V-back. Eventually the vertical eddy viscosity is thus calculated by a combination of the 3D viscosity μ-v and μ-mol, the latter being the kinematic viscosity of water, as follows: μ-v = μ-mol + max(μ-v, μ-v-back).

In D-Flow FM four turbulence closure models can be chosen, the first being user defined and the latter three based on models by Kolmogorov and Prandtl, all are explained in further detail in [Deltares, 2020, p.112-120];

1. Constant coefficient - resulting in a parabolic vertical velocity profile
2. Algebraic eddy viscosity closure model - based on the von Karman constant (κ), the bed friction (Cf), without including transport processes, computing mixing lenght (L), the shear velocity and the vertical turbulent viscosity μ-v.
3. K-ε turbulence model - involves solving a non-linear coupled system of equations describing turbulent kinetic energy (K) and energy loss (ε) including diffusivity coefficients (D), a turbulent kinetic energy production term (P), a Buoyancy flux (B) and a variation of kalibration terms (c1-3). Thereafter the the vertical eddy viscosity μ-v is determined as proportianal to the ratio K^2/ε and the mixing lenght. Still, this coupled system has to be discretized in terms of advection and diffusion which is done explicitly by a first order upwind scheme and implicitly, respectively. Accordingly the production and buoyancy term are discretized while conserving the diagonally dominant matrix (ensuring positivity). Finally this leads to two tri-diagonal matrices for K and ε that can be solved using Thomas algorithm, which may be seen as the tri-diagonal LU-decomposition, by using specific boundary conditions.
4. K-τ turbulence - Where τ is a typical timescale of the turbulent eddies and the eddy viscosity is proportional to K·τ. Coupled by a system of convection diffusion equations including diffusivity, production and buoyance terms. The resulting advection equation is discretized with an first order upwind difference scheme and the vertical diffusion term is discretized implicitly by a temporal discretization scheme. Again this leads to two tri-diagonal matrices that can be solved by the Thomas algorithm using specific boundary conditions.

B

Modelling of flow and transport

B.1. Molecular diffusion

As emphasized by [Battjes, 2017, p194]: "..molecular diffusion is irrelevant in civil engineering practice, where turbulent diffusion and dispersion are dominant..".

In this case however it could be relevant because of the specific experiment. Still with the goal of modelling the Rhine-Maas delta in mind emphasis may be put on diffusion and dispersion processes related to turbulence. Moreover it is assumed constant accross the experiment thus numerical errors can not be specifically dedicated to the diffusion.

B.2. Turbulent diffusion

To describe the turbulent diffusion the fluctuating quantaties are averaged over a certain time and lenght scale. Because of gravity the concentration gradient is positive in the downward z-direction. From the averaging of the turbulent motion and the gravity induced concentration gradient it follows, as quoted from [Vuik et al., 2007, p.197], that: "..turbulent fluctuations cause a mean transport in the direction of decreasing values of the mean concentration, as in a diffusion process."

Because the fluctuating quantities cause such net transport processes, the resulting motion and turbulent properties need to be quantified. To this end Prandtl [1925] defined the concept of mixing lenght that defines the lenght over which the fluctuations cause a deviation from the average state and correspond to the average distance the turbulence eddies travel. For example, velocity fluctuations can be related to the velocity of the turbulent eddies. Further the turbulence induced transport processes are found to be proportional to the concentration gradient, also called the turbulence diffusivity. It has the order of magnitude of the eddie velocity times the mixing lenght.

For vertical diffusion in free surface flows the mixing lenght changes over the depth since it is induced by the bed friction expressed in the bed shear stress (τ-b). Using his an estimate of the particle velocity can be made by the so-called shear velocity which together with a parabolic variation of the mixing length over the depth gives a measure for the turbulence diffusivity: $\varepsilon t = K \cdot u \cdot L = K \cdot u \cdot z \cdot (1 - z/d)$. Where K is the Von Karman coefficient which was previously empirically determined.

In exactly this manner horizontal momentum can be vertically distributed through so-called Reynolds shear stress (τ-xz). Thus, in this case it is not a concentration (c) but a momentum per unit volume (ρu) that is diffused, an effect referred to as eddy viscosity. In a simple free surface flow [Vuik et al., 2007, p.199] shows how this leads to a logarithmic velocity profile.

C

Reference models

C.1. Primary reference model

SETTINGS TABLE HERE ALL PLOTS HERE

C.2. Secondary reference model

SETTINGS TABLE HERE ALL PLOTS HERE

C.3. Tertiary reference model

SETTINGS TABLE HERE ALL PLOTS HERE

D

Modelling results

E

Observed limits of the D-Flow FM Model

E.1. Time step size
E.2. Spatial resolution